DENTAL MATERIALS 35 (2019) 1683–1694

Available online at www.sciencedirect.com

ScienceDirect

journal homepage: www.intl.elsevierhealth.com/journals/dema

Optimization of 3D bioprinting of periodontal ligament cells

Nimal Thattaruparambil Raveendran[a], *Cédryck Vaquette*[a], *Christoph Meinert*[b], *Deepak Samuel Ipe*[c], *Saso Ivanovski*[a,*]

[a] *School of Dentistry, The University of Queensland, Brisbane, QLD 4006, Australia*
[b] *Institute of Health and Biomedical Innovation, Queensland University of Technology, Kelvin Grove, QLD 4059, Australia*
[c] *School of Dentistry and Oral Health, Griffith University, Gold Coast, QLD 4215, Australia*

ARTICLE INFO

Article history:
Received 14 April 2019
Received in revised form
23 July 2019
Accepted 31 August 2019

Keywords:
3D bioprinting
Periodontal ligament cells
Gelatin methacryloyl
Cell viability
Periodontal tissue engineering

ABSTRACT

Three-dimensional (3D) bioprinting of cells is an emerging area of research but has been not explored yet in the context of periodontal tissue engineering.

Objective. This study reports on the optimisation of the 3D bioprinting of periodontal ligament cells for potential application in periodontal regeneration.

Methods. We systematically investigated the printability of various concentrations of gelatin methacryloyl (GelMA) hydrogel precursor using a microextrusion based three-dimensional (3D) printer. The influence of different printing parameters such as photoinitiator concentration, UV exposure, pressure and dispensing needle diameter on the viability of periodontal ligament cells encapsulated within the 3D bioprinted construct were subsequently assessed.

Results. This systematic evaluation enabled the selection of the most suited printing conditions for achieving high printing resolution, dimensional stability and cell viability for 3D bioprinting of periodontal ligament cells.

Significance. The optimised bioprinting system is the first step towards to the reproducible manufacturing of cell laden, space maintaining scaffolds for the treatment of periodontal lesions.

1. Introduction

The major goal of periodontal therapy is to restore the hierarchical organization of lost or impaired hard (i.e. bone and cementum) and soft tissues (i.e. gingiva and periodontal ligament) due to periodontitis. Current treatment modalities, such as guided tissue regeneration and the use of bioactive molecules, are not predictably effective in reconstituting the complex hierarchical architecture of the periodontium in most clinical cases [1,2]. As an alternative, tissue engineering has emerged as a promising strategy for periodontal regeneration [3,4].

Tissue engineering combines principles and technologies of material science, engineering and life science for the regeneration of biological tissues [5] whereby a biomimetic three dimensional porous scaffold provides a template to guide tissue regeneration. Additive manufacturing technologies such as three dimensional (3D) printing, allow accurate control over the dimensional and architectural features of the scaffolds, which is favourable for reproducing the complex hierarchical architecture of periodontal tissues [6]. Further to this, the

* *Corresponding author.*
E-mail address: s.ivanovski@uq.edu.au (S. Ivanovski).
https://doi.org/10.1016/j.dental.2019.08.114

direct printing of cells within a bioink (referred herein as 3D bioprinting) results in the manufacturing of cell-laden tissue engineered constructs with enhanced regenerative potential in a specialised and compartmentalised manner by enabling the spatially accurate delivery of multiple cell types similar to the biological composition of the periodontium. Although this technology has been used for different tissue engineering applications such as bone, cartilage, liver, cardiac, vascular and skin tissue engineering [7], its implementation for regenerative dentistry and more particularly for periodontal regeneration is still in its infancy.

Bioprinting involves the use of a bioink to entrap the cells, which is then extruded through a dispensing tip to deposit strands at defined locations. Therefore, the rheological properties of the bioink are key parameters for achieving the spatially defined and reproducible printing of cell laden scaffolds. As such, the bioink should be a thixotropic fluid (shear thinning) enabling the materials to flow under shear stress and resuming a more viscous, and ultimately solid nature once extruded. However, the difficulty of maintaining an appropriate balance between cytocompatibility and printability of the bioink is a major challenge in cell printing [8]. Indeed, low viscosity bioinks with excellent cell viability potential, upon extrusion are unable to maintain a cylindrical shape prior to crosslinking, resulting in flattening of the printed strands that greatly affects both printing resolution and macroscopic shape [9,10]. The printing quality and shape fidelity of the 3D printed construct can be improved by blending the bioink with other polymers of higher viscosity [11–13]. However, this approach remains challenging as an increase in the printing pressure is necessary to extrude the bioink, which results in higher shear forces that can be detrimental to cell viability [14–16].

Therefore, an ideal bioink should possess an appropriate flow behaviour to facilitate the manufacturing process, have a high cell affinity and should be able to retain its shape spontaneously or until chemical crosslinking. Amongst the plethora of bioinks, gelatin has been proposed as a natural biomaterial of choice due to its widespread availability, high cell affinity, and low immunogenicity. Additionally, the non-Newtonian hydrogel formed by the thermal crosslinking of gelatin at room temperature (~25 °C) can be used for microextrusion. However, the poor aqueous stability of gelatin at physiological temperature (37 °C) limits its application in cell printing as the bioprinted scaffold, if not crosslinked, does not retained its shape [17]. Therefore, different crosslinking mechanisms such as enzymatic (tyrosinase and transferase) and chemical (aldehydes, genipin and isocyanates) methods have been used to improve dimensional stability [18]. However, the high cost of enzymatic crosslinking and cytotoxicity of chemical crosslinking makes photocrosslinking more appropriate for cell printing.

Recently, a different method of crosslinking gelatin has been explored and involves the functionalization of gelatin with methacrylic groups (GelMA) which can be subsequently photopolymerized using cytocompatible photoinitiators such as Irgacure 2959 (IC 2959, 1-[4-(2-hydroxyethoxy)-phenyl]-2-hydroxy-2-methyl-1-propanone) and lithium phenyl-2,4,6-trimethylbenzoylphosphinate (LAP) [19–21]. These strategies result in rapid crosslinking and enhanced thermal stability of the 3D-printed GelMA constructs, which are favourable properties for utilization in the tissue engineering of various structures, including the periodontium [19].

Prior to *in vivo* utilization, the 3D bioprinting of periodontal ligament cells using GelMA needs to be optimised by controlling different parameters, such as printing pressure, collector speed, nozzle inner diameter, polymer concentration, photoinitiator type/concentration, temperature, printing offset and viscosity of the bioink, in order to obtain the deposition of uniform and continuous strands [22]. The viability of the printed periodontal ligament cells is another factor that must be considered while optimising a printing technology. Many of the aforementioned parameters, especially bioink concentration/viscosity, printing pressure and temperature and diameter of the nozzle, have a significant influence on the amount of shear force acting on the cells during extrusion, which affects their viability.

The objective of this study was to optimise a 3D bioprinting strategy for human primary periodontal ligaments cells (PDLCs) using GelMA hydrogels, for potential future utilization in periodontal tissue engineering applications.

2. Materials and methods

2.1. *Periodontal ligament cell (PDLCs) culture*

Human primary PDLCs were isolated from the periodontal ligament of an extracted tooth using a previously reported method [23]. Institutional approval for the use of these cells were granted by Griffith University under approval number DOH/07/13/HREC. The cells were cultured at 37 °C and 5% CO_2 in Dulbecco's Modified of Eagle's Medium (DMEM, Life Technologies, Australia) supplemented with 10% (vol/vol) fetal bovine serum (FBS from Gibco®, Australia), 1% (vol/vol) non-essential amino acids and 1% (vol/vol) Penicillin–Streptomycin–Glutamine (Gibco®, Australia).

2.2. *Preparation and characterization of gelatin methacryloyl (GelMA)*

Porcine type A gelatin with 250 bloom (Gelita, Germany) was functionalized by following a previously published protocol [19]. Briefly, gelatin was dissolved at 10% (w/v) in sterile phosphate-buffered saline (PBS) at pH 7.4 and 50 °C and reacted with 0.6 g methacrylic anhydride (Sigma-Aldrich, Australia) per gram of gelatin for 1 h under constant stirring. The reaction mixture was then transferred to dialysis tubing of 12-kDa MWCO (Sigma-Aldrich, Australia) and dialysed against ultrapure water at 40 °C for 5 days. The pH of the dialysed GelMA solution was adjusted to 7.4 using 1 M sodium bicarbonate (Sigma-Aldrich, Australia) and the solution was sterilized using 0.2 μm syringe filters. The filtrate was freeze-dried and stored at −80 °C for further use.

Methacryloyl-functionalization of GelMA was investigated using proton nuclear magnetic resonance (^{1}H NMR) performed with a Bruker Avance 600 MHz spectrometer (Bruker, USA) at room temperature and 1% (w/v) macromere concentration in 90% H_2O/10% D_2O. The degree of functionalization (DoF)

was quantified using a 2,4,6-trinitrobenzenesulfonate (TNBS) assay (Sigma-Aldrich, Australia) as previously described [24].

2.3. Rheological properties of GelMA

The rheological properties of 5, 10, 12.5, 15 and 20% (w/v) GelMA hydrogel precursor solutions were evaluated using an Anton Parr M302 rheometer with a stainless steel upper cone plate of 25 mm diameter and 1° cone angle with a gap of 0.05 mm between the lower flat surfaces at 25 °C. The Linear Visco Elastic Region (LVER) of different samples were determined using an amplitude sweep, where the storage modulus (G′) and the loss modulus (G″) at different shear strain (0.01–1000%) and constant frequency (10 s^{-1}) were measured.

The flow behaviour of the gel systems was evaluated using flow curve analysis. The changes in the viscosity of the hydrogel precursor with the increase of shear rate (0.1–1000 s^{-1}) at 25 °C was measured and plotted as a flow curve. The rheological curves were used to interpret the flow behaviour of GelMA which is essential for microextrusion-based printing [8].

2.4. Optimization of printing parameters

The impact of the rheological properties of the bioink on printing was evaluated using 5, 10, 12.5 and 15% (w/v) GelMA solutions in sterile PBS at 37 °C. After thorough mixing the hydrogel precursor solutions were incubated in a 37 °C water bath for 10 min and centrifuged at 3000 *rpm* for 2 min to remove entrapped air bubbles. Thereafter, the hydrogel precursor solution was transferred to the printing cartridge and allowed to cool to room temperature (~25 °C) for 20 min to allow thermal crosslinking. Tapered dispensing tips (25 or 27 G) were connected to the cartridge and the bioink was 3D printed using a BioScaffolder 3.1 (GeSiM, Germany). Extrusion of the hydrogel precursor solution was performed by applying a range of pressures (0–600 kPa) to determine the minimum pressure enabling consistent flow of the bioink through the printing dispensing tip. In addition, a range of printing speeds (5–20 mm/s) were used in order to assess the effect on printability and strands morphology. The strand thickness of the 3D printed scaffolds was measured from optical microscopy images using Image J software.

2.5. Dissolution of 3D printed scaffolds

The efficiency of UV crosslinking was investigated by measuring the degree of dissolution of 3D printed scaffolds in PBS at 37 °C. To this end, the 12.5% (w/v) GelMA solution was selected from the previous experiment and mixed with different concentrations of photo-initiators (0.01, 0.05, 0.10, 0.15, 0.30 and 0.50% (w/v)) for Irgacure 2959 (IC 2959, 2-hydroxy-4′-(2-hydroxyethoxy)-2-methylpropiophenone from Sigma-Aldrich, Australia) and (0.01, 0.05, 0.10% (w/v)) for LAP (Lithium Phenyl (2,4,6-trimethyl benzoyl) phosphinate from Tokyo Chemical Industry Co., Ltd, Japan). The dimensions of the printed scaffolds were 5 mm × 5 mm with 4 layers and 0.8 mm fibre spacing. Immediately after printing, the scaffolds were exposed to UV irradiation (320–500 nm) of 10 W/cm^2 (OmniCure® S1500, Germany) at 35 mm offset for different times (2, 5, 10, 20 and 30 s). To assess the stability of the scaffolds, immediately after crosslinking, they were weighed (Wi) (3 scaffolds per crosslinking time), transferred to 1 ml sterile PBS in a 24 well plate and placed at 37 °C in a cell culture incubator for 24 h. Thereafter, the scaffolds were collected and blotted on a filter paper and the weight was measured (Wf). The weight loss in percentage was calculated using following equation.

$$\%\,Weight\,Loss = \frac{Wi - Wf}{Wi} \times 100$$

In addition, the scaffolds were imaged using optical microscopy in order to quantitatively determine the changes in fiber diameter using ImageJ.

2.6. 3D bioprinting of PDLCs and printing optimization based on cell viability

Based on the dissolution study and printing optimization, we selected 12.5% (w/v) GelMA, 0.05% LAP (w/v), and 20 s UV exposure at an offset of 35 mm for 3D bioprinting. The impact of LAP, UV photopolymerization, printing pressure and various inner diameters of the dispensing tip (using tapered needles from 14 G to 27 G) upon cell viability was systemically investigated.

To this end, 2×10^6 PDLCs were resuspended in 1 ml of 12.5% (w/v) GelMA in PBS at 37 °C, and 20 μl of the cell-laden bioink was drop-cast on a petri plate and thermally crosslinked at 24 °C for 20 min and used as a positive control. In order to assess the potential toxicity of the photo-initiator, 20 μl of the cell laden GelMA with 0.05% LAP was drop-cast and thermally crosslinked only (no UV). In order to assess the potential toxicity of UV exposure in conjunction with the presence of LAP, the specimens similar to the two previous groups were also exposed to UV irradiation (320–500 nm) of 10 W/cm^2 for 20 s at a 35 mm offset. The impact on cell viability of the printing pressure was assessed with the 12.5% cell laden GelMA without LAP or UV-exposure, utilising a printing pressure of 240 ± 10 kPa and printing head translation speed of 11 ± 1 mm/s through a 27 G dispensing tip. Hence, 5 different groups were created: (1) casted cellular solution in GelMA (Control), (2) Control with 0.05% LAP (with LAP), (3) control with a 20 s UV-exposure (with UV), (4) control with 0.05% LAP and with a 20 s UV-exposure (with LAP & UV), (5) the bioprinted cellular GelMA (Printed) without LAP or UV irradiation. The specimens of groups (1) Control, (2) with LAP, (3) with UV and (5) Printed were maintained at room temperature (23 °C) in order to prevent dissolution of the uncrosslinked GelMA, thus allowing for the immediate staining of living and dead cells. Group (4) with LAP & UV was utilised to evaluate potential late toxicity of the photo-initiator and the UV. To this end, the specimens of this group were immersed in 1 ml of medium and further cultured in an incubator (37 °C, 5% CO_2) for 24 h. Cytotoxicity was assessed by performing a Live/Dead assay according to the following protocol: the cell laden hydrogels were incubated at room temperature (to prevent the dissolution of the GelMA) with 5 μg/ml of fluorescein diacetate (FDA, Sigma-Aldrich, Australia) to visualize the live cells, and 2 μg/ml of propidium iodide (PI, Sigma-Aldrich, Australia) to stain the dead cells, in PBS for 30 min.. The samples were imaged at room temperature using a Nikon eclipse Ti confocal

Microscope at Exc/Em 488/526 for FDA and Exc/Em 493/636 nm for PI. For each group 3 scaffolds were utilised (3 scaffolds with 3 images each).

The influence of different inner diameter of the dispensing tips on the cell viability of the printed scaffolds was also evaluated. The bioink (12.5% (w/v) GelMA with 0.05% (w/v) LAP) containing 2×10^6 PDLCs was extruded through 14, 16, 18, 20, 22, 25 and 27 G (1600, 1194, 838, 603, 413, 260 and 210 μm inner diameter, respectively) dispening tips at 240 kPa. The extruded bioink was further UV crosslinked for 20 s at 35 mm offset. As a positive control, 20 μl of cell laden bioink with LAP was drop cast and UV irradiated. Immediately after crosslinking, samples were stained using the Live/Dead assay as described above.

In addition, PDLCs viability was assessed over 14 days of culture. To this end, 2×10^6 cells were resuspended in 1 ml of bioink (12.5% (w/v) GelMA with 0.05% (w/v) LAP in PBS) at 37 °C and immediately transferred to a sterile 10 ml cartridge, sealed using a plunger and allowed to thermally crosslink for 20 min at room temperature, and subsequently printed and crosslinked using the optimised parameters (25 G dispensing tip, 135 ± 15 kPa printing pressure, 11 ± 1 mm/s printing speed, 20 s UV exposure at 35 mm offset). Immediately after UV crosslinking, the scaffolds were transferred to cell culture medium in 24 well plates. The scaffolds were incubated in a 37 °C and 5% CO_2 humidified cell culture incubator for up to 14 days and the culture medium was changed every 3 days. The viability of the cells entrapped in the scaffolds was studied using the Live/Dead assay at day 0, 1, 3, 7 and 14 according to the method described above. For all experiments, the number of green and red cells in the confocal images (3 scaffolds with 3 images each) were determined using ImageJ software as we previously reported [25]. The green and red channels were isolated, binarised and the threshold was adjusted in order to remove the background. Thereafter the function in ImageJ called 'Analyse Particles' was utilised to count cells from each channel. The cell viability (%) was quantified using the following formula:

$$\textit{Cell vibility}\ (\%) = \frac{\text{Total number of green cells}}{\text{Total number of green and red cells}} \times 100$$

2.7. Statistical analysis

The statistical difference between the groups were analysed by one-way ANOVA followed by a Tukey post-hoc analysis using GraphPad Prism 7 software. A probability level (p) less than 0.05 considered as significant and represented with *, ** and *** when $p < 0.05$, $p < 0.01$ and $p < 0.001$ respectively. When only two groups were compared a t-test was utilised in order to determine the statistical significance ($p < 0.05$).

3. Results

3.1. GelMA synthesis and characterization

First, we performed proton nuclear magnetic resonance (^{1}H NMR) analysis to confirm successful functionalization of gelatin with methacryloyl groups (Fig. 1A). As expected, the ^{1}H NMR spectra of GelMA displayed distinct peaks in the 5–6 ppm range (a + b) corresponding to acrylic protons of methacryloyl groups grafted to lysine and hydroxylysine residues of the gelatin backbone. Further confirming this finding, the peak corresponding to methylene protons of lysine groups at approximately 2.9 ppm (c) was reduced in GelMA compared to gelatin and the GelMA spectrum displayed a distinct peak corresponding to methyl protons of methacryloyl groups at approximately 1.8 ppm (d). Functionalization of gelatin can occur at primary amines and hydroxyl groups. Since peaks corresponding to methacrylate groups were not detected in the ^{1}H NMR spectrum of GelMA (expected at approximately 6.1 ppm), we chose a to quantify the degree of functionalization using a 2,4,6-trinitrobenzene-sulfonic acid (TNBS) assay, which indicated that 70 ± 6% of primary amines were functionalized with methacrylamide groups.

3.2. Rheological properties of GelMA

The storage modulus (G′) and viscous modulus (G″) of 5, 10, 12.5, 15 and 20% (w/v) GelMA hydrogel precursors at different shear strain are represented in Fig. 2A.

All of the hydrogel precursors had higher G′ than G″, suggesting that the gel precursors have more elasticity than viscosity. The G′ and G″ of the GelMA hydrogels precursors increased with the increase in GelMA concentrations. G′ and G″ at 0.1% shear strain increased from 60 Pa and 5 Pa to 5000 Pa and 200 Pa respectively, when the GelMA concentration raised from 5% (w/v) to 20% (w/v). Fig. 2A shows that G′ and G″ remained constant for a particular period of shear strain (G′ plateau), but at higher shear strain the G′ values dropped. At the same time, G″ value increased indicating that the GelMa was behaving more similarly to a liquid.

The viscosity of the hydrogel precursor is another property that needs to be considered for extrusion-based 3D bioprinting. The viscosities of the hydrogel precursors were measured from 0.1 to 1000 s^{-1} of shear rate and the obtained flow curves are represented in Fig. 2B. Similar to G′, the viscosity of the hydrogel precursors increased with GelMA concentration. The viscosity of 5% (w/v) GelMA at 1 s^{-1} was 9.7 Pa s and this increased to 200 Pa s when the concentration rose to 20% (w/v). Fig. 2B shows that the viscosity of all of the hydrogel precursors decreased gradually with increase in shear rate indicating a flow behaviour under high shear, which made the hydrogel precursors suitable for extrusion.

3.3. Optimization or printing parameters

The printability of the various concentrations of GelMA (5–20% (w/v)) was investigated through 25 and 27 G dispensing tips using the GeSiM BioScaffolder 3.1. The applied pressure to the extruders and the translation speed of the extruder were optimised in order to obtain consistent flow of GelMA and continuous prints. As seen in Table 1, the minimal pressure for enabling printing increased with the higher GelMA concentrations, which correlates with the rheology data as higher viscosity required higher pressure to allow the bioink to flow. The printing pressure also increased with the decrease in the inner diameter of the dispensing tip indicating that there was a higher shear stress in the smaller diameter tips which

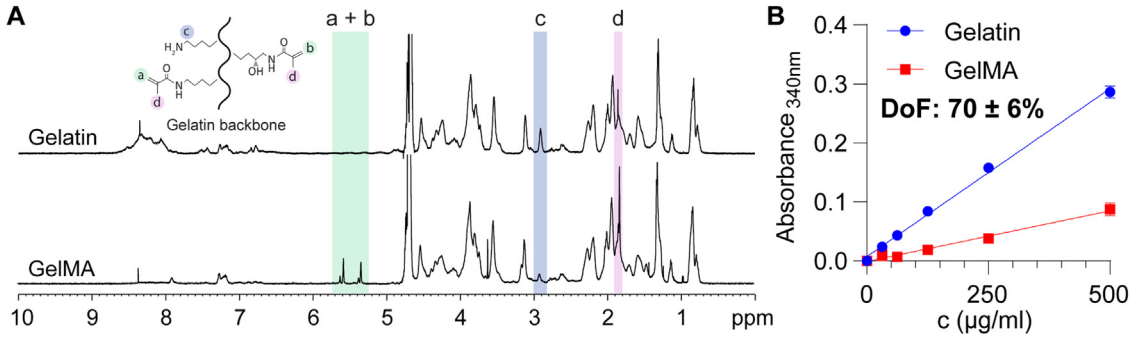

Fig. 1 – Characterization of gelatin and GelMA. ^{1}H NMR spectra of gelatin and GelMA demonstrating successful functionalization of lysine and hydroxylysine residues with methacrylamide groups (A), and quantification of the degree of functionalization (DoF) determined using a 2,4,6-trinitrobenzene-sulfonic acid (TNBS) assay (n = 2 independent measurements; mean ± STDEV) (B).

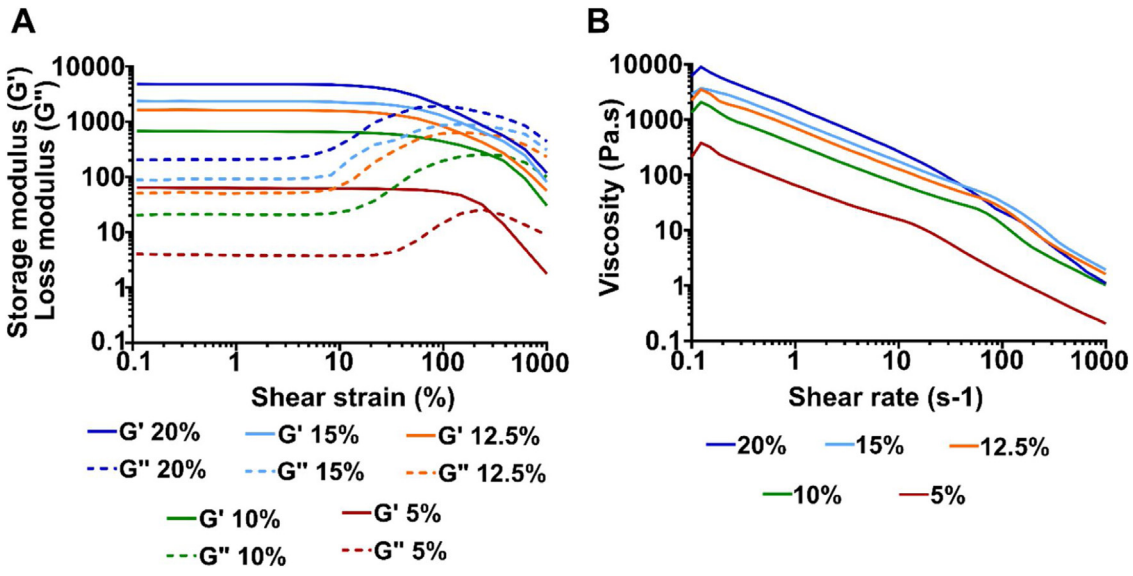

Fig. 2 – Rheological characterization of GelMA hydrogel precursors G′ and G″ of GelMA hydrogels at different shear strains (A), and flow curve of GelMA hydrogels at different concentrations (B).

Table 1 – Printing optimization parameters of hydrogel containing different concentrations of GelMA through 25 and 27 G dispensing tips.

GelMA concentration (w/v)	Printability (Yes/No)	Printing pressure (kPa)	Printing speed (mm/s)	Strand thickness (μm)
25 G dispensing tip at room temperature				
5	No[a]	–	–	–
10	No[a]	–	–	–
12.5	Yes	120–150	10–12	551 ± 52
15	Yes	250–280	8–10	643 ± 25
20	No[b]	–	–	–
27 G dispensing tip at room temperature				
5	No[a]	–	–	–
10	Yes	160–200	5–8	430 ± 37
12.5	Yes	230–250	10–12	381 ± 29
15	Yes	420–450	8–10	513 ± 65
20	No[a]	–	–	–

[a] Less viscous, extruded as liquid even at low pressure (50 kPa).
[b] Highly viscous, no extrusion even at the maximum possible pressure of 700 kPa of the 3D printer used.

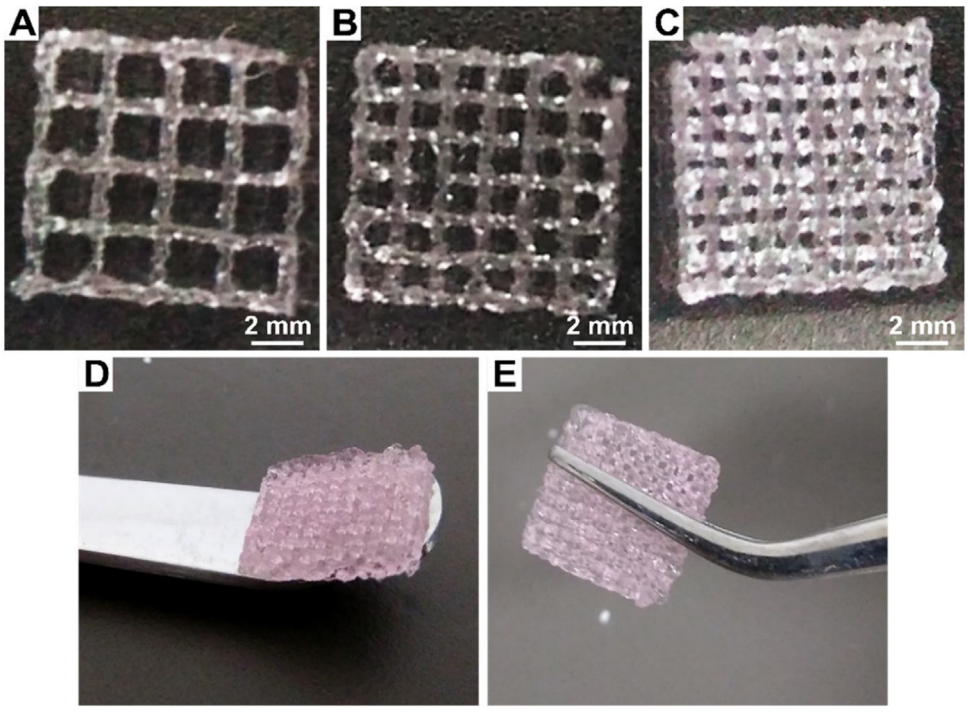

Fig. 3 – Thermally crosslinked 3D-printed GelMA hydrogel with different pore sizes (179.5 ± 9.4, 94.4 ± 9.3, and 47.0 ± 8.7 μm, respectively) (A–C), and physical handling of the scaffold with surgical spatula and forceps (D & E).

prevented extrusion at lower pressures. In addition to the interplay between GelMA concentrations and extrusion pressure, the translation speed of the extruder had to be adjusted for each condition in order to fabricate homogenous scaffolds with consistent strand diameter, as shown in Table 1.

We observed that the 5% (w/v) GelMA was not suitable for printing, even with a very low pressure of 50 kPa, as the material was extruding in the form of liquid droplets from the dispensing needle that rapidly spread on the printing platform. A higher concentration of 10% (w/v) improved the printability and GelMA printing was possible with a 27 G dispensing needle at 5–8 mm/s but the printing repetitively failed after the extrusion of 10 struts. However, an increase in GelMA concentration to 12.5% (w/v) drastically changed the printability of the bioink and a continuous printing with a homogeneous strand diameter could be achieved regardless of the scaffold pore size (Fig. 3A–C). Further increasing the GelMA concentration resulted in a similar impact on printability, although this required higher extrusion pressures which can be detrimental to cell viability. From these results, we selected 12.5% (w/v) GelMA for further investigation. The photocrosslinked 3D-printed scaffolds using 12.5% GelMA possessed sufficient physical integrity while handling with forceps and a surgical spatula (Fig. 3D, E).

3.4. *Physical stability of 3D printed scaffolds*

The stability of 3D-printed scaffolds in the aqueous medium is an important parameter for medical applications and therefore a systematic evaluation of the effect of photoinitiator concentrations and length of UV-irradiation (used for the crosslinking) was performed. Fig. 4A & B shows the aqueous stability of IC2959- and LAP-crosslinked GelMA scaffolds at 37 °C. This demonstrated that 0.01% (w/v) of both photoinitiators were not sufficient to induce crosslinking as 100% weight loss was observed 24 h post-immersion in PBS. Subsequently, as the photoinitiator concentrations increased, the subsequent weight loss decreased, indicating that a higher degree of crosslinking resulted in increased thermal stability. Interestingly, LAP was a much more efficient photo-initiator compared to IC 2959 as enhanced stability was obtained with lower concentrations and UV-irradiation exposure. As a result, IC2959 concentrations higher than 0.3% (w/v) with more than 10 s of UV exposure were necessary in order to obtain a stable printed scaffold, whereas a low concentration of LAP 0.05% (w/v) provided stable gel structures for similar UV exposure times (Fig. 4B). In addition to the concentration of photoinitiator, the duration of UV exposure had a significant impact on the stability of the resulting scaffold. As the exposure time increased, the weight loss followed an invert trend leading to enhanced stability.

In addition to the weight of GelMA hydrogels during the immersion in PBS, the changes in strand diameter was also monitored for the GelMA-LAP system (Fig. 4C). As expected, lower concentrations of LAP caused a drastic decrease in fibre thickness due to the removal of the non-crosslink GelMA, whereas the higher concentrations of photoinitiators enabled better thermal stability resulting in reduced dimensional changes.

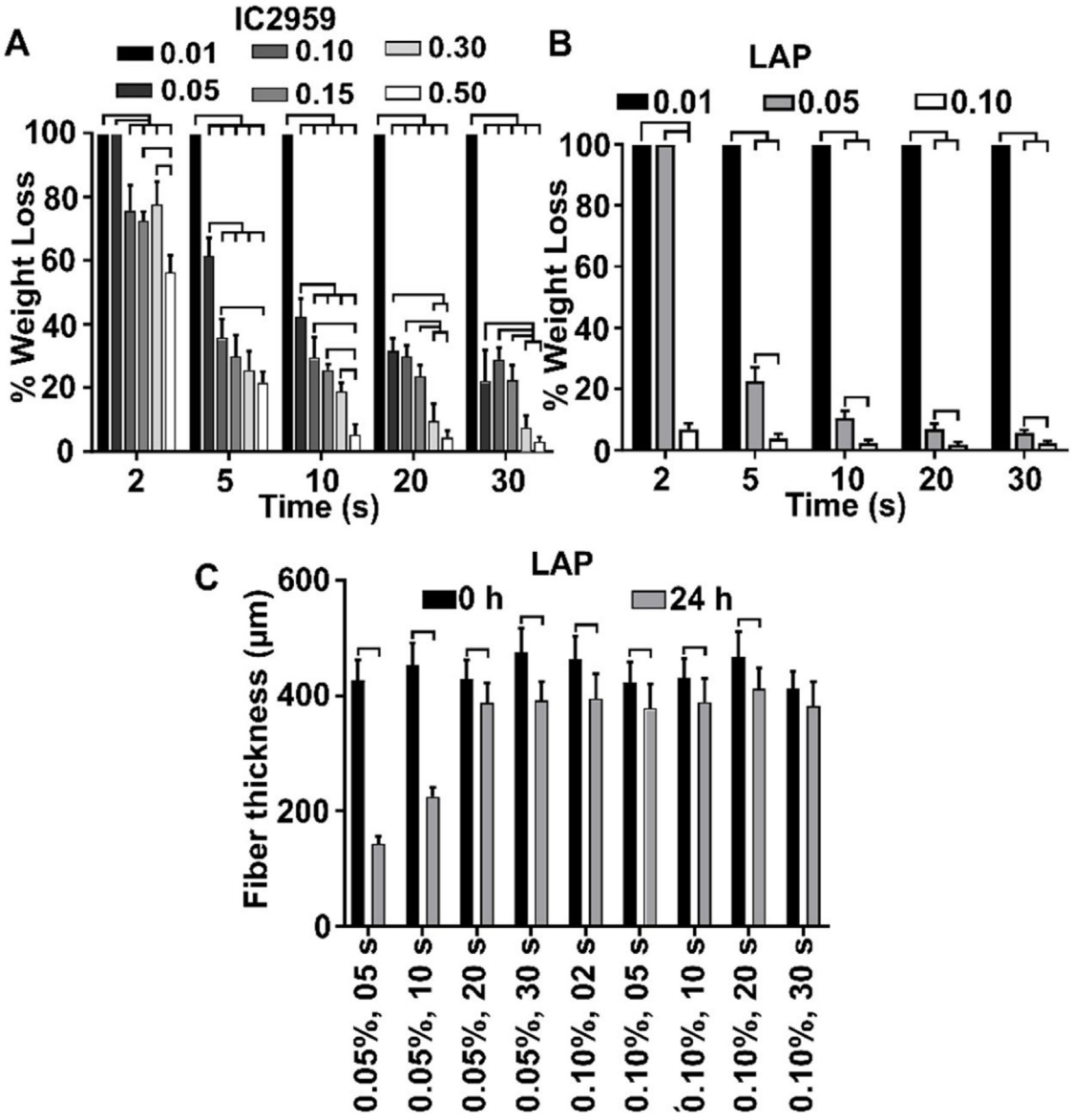

Fig. 4 – Stability of 3D printed GelMA scaffolds: Dissolution of GelMA at different concentrations of IC2959 and LAP respectively (A & B) and for various UV-exposure time, and the changes in printed filament thickness after 24 h incubation with different concentrations of LAP (C). *(n = 3 independent measurements; mean ± STDEV)*. Bars indicate statistical differences ($p < 0.05$) as measured per one way ANOVA (A and B) or using a t-test (C).

3.5. *3D bioprinting of PDLCs and printing optimization based on cell viability*

Based on the systematic assessment of the printing parameters, the printing conditions selected for the cell viability studies were 12.5% (w/v) GelMA through a 27 G dispensing needle using a 240 ± 10 kPa printing pressure at 11 ± 1 mm/s printing speed. To understand the effect of various bioink parameters on cell viability, we firstly assessed the impact of the LAP concentration of cell viability, initially without printing. The cells were mixed with GelMA with or without LAP (0.05% (w/v)) and casted onto a plate. The results indicated that LAP, at this concentration, did not induce significant toxicity (Fig. 5B). Further, we demonstrated that the optimised UV exposure did not induce any cytotoxicity in the irradiated cells in GelMA (casted not printed) in the absence of LAP. Here again, no toxic effect could be noted (Fig. 5C). Thereafter, LAP and UV-irradiation were combined on casted GelMA samples, in order to assess their impact in cell toxicity, which showed no significant cytotoxicity (Fig. 5D). Finally, the influence of printing pressure (240 ± 10 kPa) through 27 G dispensing tip on cell viability in the absence of LAP and UV-irradiation was tested and a significant effect was observed (Fig. 5E & F). The minimal pressure necessary for extruding GelMA is directly related to the dispensing tip inner diameter and the amount of shear stress that the gel experiences when being extruded. Therefore, we systematically investigated a range of tip diameters as shown in Fig. 6, which demonstrated that cells printed through

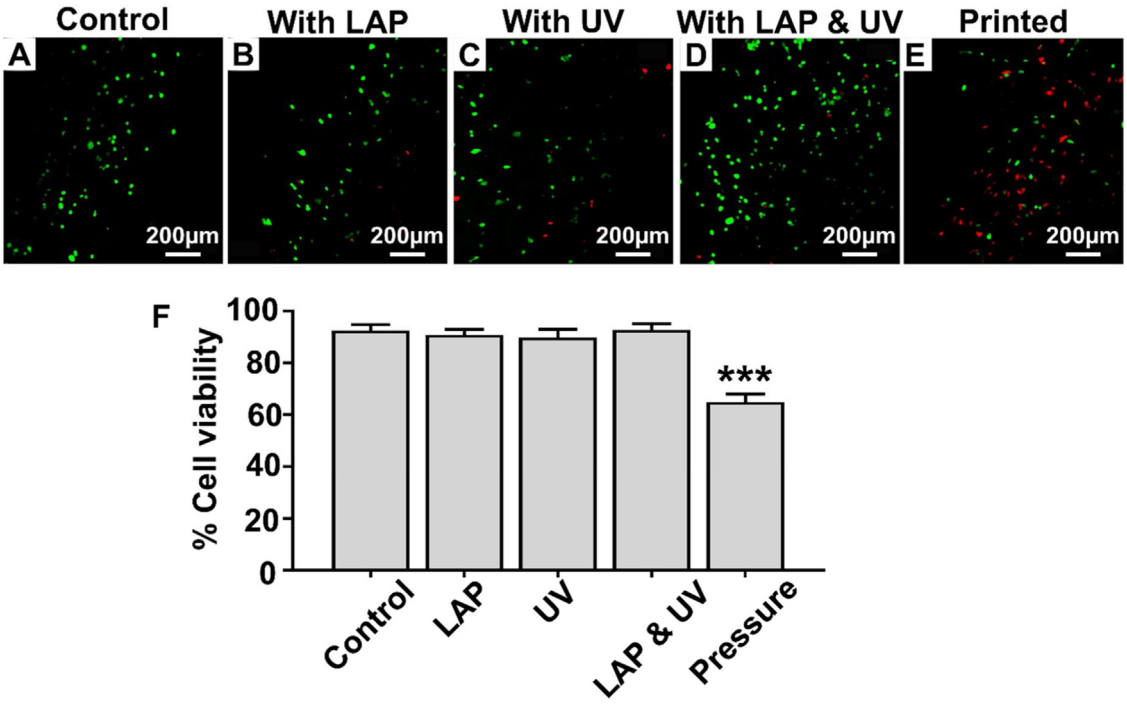

Fig. 5 – Live/ead images of control and bioink with different test parameters: Green cells are viable and red cells are dead (A–E), and % cell viability from Live/Dead confocal images using ImageJ (F). *(n = 9 measurements from 3 different constructs; mean ± STDEV)* (For interpretation of the references to color in this figure legend, the reader is referred to the web version of this article).

dispensing tips of 14, 16, 18, 20, 22 and 25 G (Inner diameter of 1600, 1194, 838, 603, 413 and 260 μm, respectively) at a similar pressure (240 kPa) did not show any significant toxicity. In contrast, the cell viability of 3D-printed PDLCs drastically decreased to 52.3 ± 6.2% when a 27 G (Inner diameter = 210 μm) dispensing tip used (Fig. 6H & I).

Fine strands are required for high printing resolution and for the mitigation of oxygen and nutrient diffusional issues that potentially impact cell viability. Therefore, a 25 G needle was selected and utilised for the remainder of the experiment. The long-term effect on the cells in the printed construct was assessed over 14 days and high levels of cell viability were observed at all-time points (Fig. 7). This was also confirmed by counting the viable green cells and dead red cells in the confocal microscopic images (n = 9, 3 images from 3 scaffolds), which showed high cell viability indicating that the cells had access to sufficient oxygen and nutrients. Despite a statistically significant decrease in the cell viability at day 7, this parameter was always above 70% indicating high cell survival throughout the 14 days of culture. In addition, it was noted that the cells started elongating from day 3 and the scaffold was densely populated with cells by day 14. The qualitative cell proliferation over 14 days of culture further confirmed the cytocompatibility of the bioink.

4. Discussion

3D bioprinting has become very popular for tissue engineering applications, however this technology has not been applied towards periodontal tissue engineering. The optimization of a suitable printing technology for PDLCs is one of the major challenges hindering the implementation of this technology for periodontal tissue engineering. In the present study, various parameters affecting GelMA printability were investigated in order to select the printing conditions required for achieving high printing resolution, shape maintenance and high PDLCs viability. To the best of our knowledge, no previous studies have reported 3D bioprinting of periodontal ligament cells. Thus, this research establishes the basis of PDLCs bioprinting and will pave the way towards further in-depth investigations of the biological response and regenerative potential of these constructs for periodontal regeneration.

Bioprinting resolution and shape fidelity relies principally on the rheological properties of the bioink that is being utilised. Generally, a compromise between printability and cell viability is required in order to reproducibly manufacture cell-laden constructs which can exert their scaffolding function while enabling cell proliferation and differentiation. Therefore, the development of a bioink capable of high printability while enabling high cell viability is of paramount importance for tissue engineering applications. As such, GelMA alone is generally a poorly printable biomaterial for microextrusion based 3D bioprinting, however innovative solutions have been implemented in order to enhance the printability without greatly affecting the cytocompatibility [26–28].

The flow behaviour of the bioink is an important property that determines its ability to be extruded through the dispensing tip [29]. As the pressure applied to the bioink increases, the viscosity decreases, thus enabling the flow of

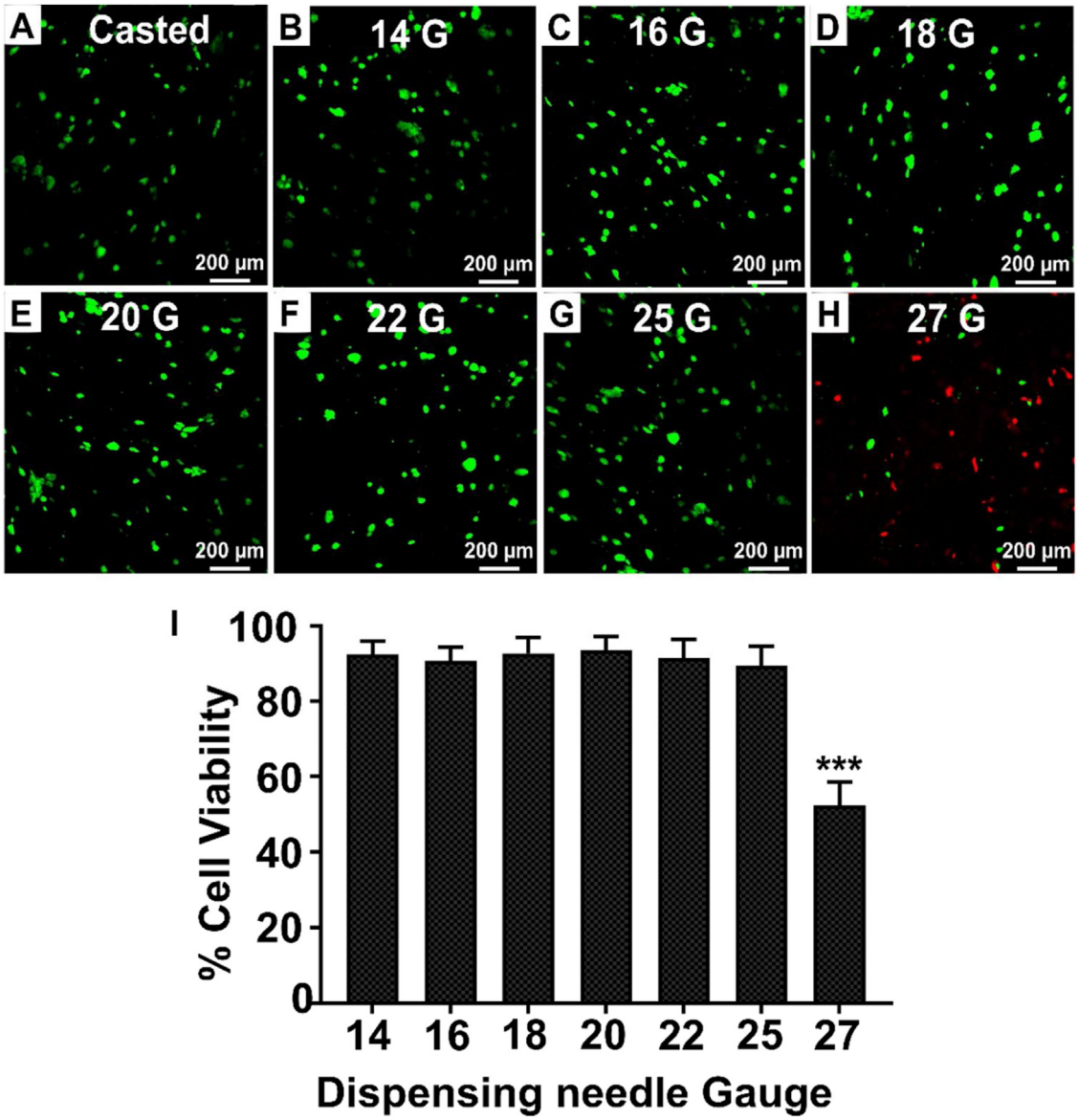

Fig. 6 – Live/ead images of the cell in casted gel and extruded through dispensing tip with different inner diameter/gauge: Green cells are viable and red cells are dead (A–E), and cell viability from Live/Dead confocal images using ImageJ (I). (*n* = 9 *measurements from 3 different constructs; mean* ± *STDEV*) (For interpretation of the references to color in this figure legend, the reader is referred to the web version of this article).

bioink through the dispensing needle. The rheological properties of the different concentrations of GelMA were investigated in order to determine the suitability of the thermally gelled bioink for microextrusion-based 3D printing. All of the tested hydrogel precursors possessed a predominantly solid character ($G' > G''$), which is necessary for maintaining the structural integrity upon printing [8,30]. Such gels only flow when exposed to external pressure which helped to retain the material in a gelled state, thus preventing uncontrolled flow of the materials when no pressure is applied or when printing is paused. Higher GelMA concentrations can reduce the effect of gravity and surface tension mediated sagging or collapse of 3D printed fibers [31,32]. However, increasing the storage modulus is detrimental to cell viability, as a higher pressure, and hence increased shear forces, is required for achieving extrusion [17]. While our approach was to find a suitable balance between the rheological properties and cell viability, other investigators have developed innovative solutions while using low viscosity GelMA solutions. Indeed, Liu et al. incubated a cell-laden 3–5% GelMA hydrogel at 4 °C for achieving thermal crosslinking and bioprinted this bioink at 21 °C with promising cell survival outcomes [33]. However, the sudden transition from 4 °C to 21 °C used for the printing could result in a poorly controlled temperature increase within the cartridge affecting the bioink viscosity in a time-dependant manner, hence leading to heterogeneous printing. Another approach involved the mixing of a low concentration of GelMA (5% (w/v)) with 8% (w/v) gelatin in an attempt to increase the

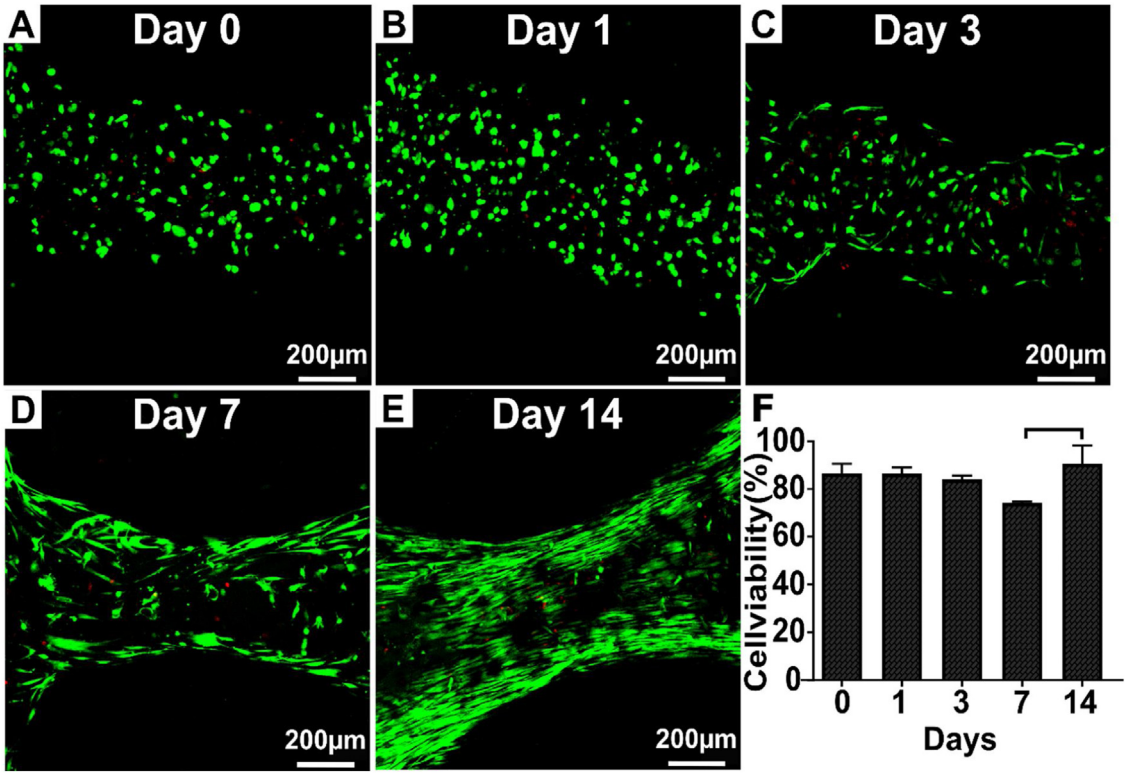

Fig. 7 – The viability of PDLCs in the 3D printed construct on Day 0, 1, 3, 7 and 14: Green cells are viable and red cells are dead (A–E), and % cell viability from Live/Dead confocal images using ImageJ (F). (*n = 9 measurements from 3 different constructs; mean ± STDEV*). The bar indicates a statistical difference ($p < 0.05$) as measured per one way ANOVA (For interpretation of the references to color in this figure legend, the reader is referred to the web version of this article).

viscosity and enhance the printability properties of the resulting bioink. After photo-crosslinking, the gelatin was leached out at physiological temperatures in order to obtain a loose GelMA network, a desirable feature for enhanced nutrient and oxygen diffusion. While the printability was greatly improved, a significant mass loss (~12%) occurred which greatly affected the mechanical properties, resulting in a very weak scaffold [28]. Therefore, the selection of a suitable concentration of GelMA for bioprinting may still be advantageous over other strategies. Our study demonstrated that a 12.5% (w/v) GelMA concentration was optimal, as it enabled printing at reasonable pressure while still maintaining cell viability and enabling cell proliferation. In addition, higher GelMA concentrations of 15% and 20% (w/v) can be an obstacle for mixing cells into the bioink due to the formation of air bubbles, which can potentially lead to printing disruption and clogging of the dispensing needle [34].

The pressure applied during printing is also an important parameter as it affects the level of shear that the cells are experiencing, the amount of bioink extruded per time unit, and ultimately the internal architecture of the 3D-printed scaffold. As the applied pressure increases, the fiber thickness also increases, and as the printing speed increases, the fiber thickness decreases, as previously reported [22,35]. Fibers with a small diameter are generally preferred as this implicitly means that the printing resolution is enhanced [22], and they are more favourable for oxygen and nutrient diffusion. Even though we used dispensing needles with very small inner diameter (260 and 210 μm), the fiber thicknesses were significantly higher than the inner diameter. As the bioink is extruded through the narrow orifice dispensing tip, the GelMA polymer chains in the hydrogel are compressed and aligned to facilitate extrusion. However, when the bioink is dispensed, the pressure within the hydrogel drops and results in loosening of the polymeric chains, which resulted in increased fiber thickness [36,37].

After optimising the printing parameters, the next challenge was to find the most suitable concentrations of IC2959 and LAP for photo crosslinking of GelMA. When subjected to temperature lower than 25 °C, pure (without crosslinkers) GelMA polymers can undergo reversible coil helix transition by intermolecular bonds and form a thermo-responsive hydrogel. However, an increase in temperature weakens the polymeric crosslinks and results in the transition from gel to liquid. Therefore, photocrosslinking is required in order to ensure irreversible crosslinking of the methacrylated gelatin chains which leads to appropriate dimensional stability at physiological temperature while still maintaining good cytocompatibility [38–40].

In addition to dimensional stability, cell viability of the scaffolds is another challenge in 3D cell printing. During microextrusion printing, cell viability can be affected by various parameters: printing pressure and consequential shear stress, potential toxicity from the photo-initiator,

excessive exposure to UV, and radical formation during the photopolymerization reaction. We demonstrated that a low concentration of LAP, combined with short UV-exposure, did not induce any significant toxicity. On the contrary, the pressure required to extrude the hydrogel through a 27 G dispensing needle caused significant cell death. The lack of stress shielding properties of GelMA result in the exposure of the cells to excessive shear and induced cell death. Indeed, the PDLCs printed at a printing pressure of 200 kPa through a 27 G dispensing tip resulted in 64.9 ± 3.1% cell viability, which was consistent with a previous report, albeit for a different cell type [36]. The shear stress at the dispensing tip can be decreased by increasing the temperature (that is lowering the viscosity) or increasing the inner diameter of the tip [41]. In our current study, we evaluated the influence of different tips on cell viability and found consistently high cell viability up to a certain inner diameter threshold, after which most cells were dead. Here again, a balance between printability, printing resolution and cell viability is needed, therefore the 25 G tip presented the most satisfactory results when all of these criteria were considered.

The PDLCs printed in the GelMA construct remained circular for 1 day, and then started spreading before resuming a fully elongated morphology typical of this cell type, which confirmed the long-term cytocompatibility of GelMA and suggested that the stiffness of the gel was suitable for cell proliferation and migration. Possibly for this reason, the printed constructs that were manufactured in this study featured earlier cell spreading at day 7 compared to that of cells printed using different gelatin based bioinks [28,42,43]. Microscopic imaging suggested that PDLCs proliferated in the 3D-printed construct and colonised the entire structure by day 14, without the development of a necrotic core. Importantly, the crosslinked GelMA construct retained its physical integrity and displayed excellent dimensional stability throughout the *in vitro* culture.

Taken together, the findings of the study highlight the need for appropriate optimization of cell laden bioinks in order to achieve high printing resolution, excellent dimensional stability and high PDLCs viability. The findings may also be relevant towards the bioprinting of other oro-dental mesenchymal cells, such as osteoblasts, gingival and pulp derived cells.

5. Conclusion

The present study systematically investigated various printing conditions, including GelMA concentrations, printing pressure, orifice of the dispensing tip, concentration of photoinitiator and time of UV-exposure. It was demonstrated that the best printing outcome was obtained using a 12.5% GelMA solution with 0.05% LAP (w/v) extruded at 135 kPa through a 25 G dispensing needle and UV-crosslinked for 20 s. These conditions were suitable for high resolution bioprinting that supported a high level of PDLCs viability and facilitated cellular proliferation within the GelMA construct over 14 days. This study establishes a proof of concept for the feasibility of utilising PDLCs in 3D bioprinting. Further investigation of the bioactivity of the printed cells, their biological response along with their *in vivo* efficacy is needed for advancing this concept towards clinical translation.

Acknowledgment

N. T. R. thanks the University of Queensland for his PhD scholarship.

REFERENCES

[1] Pihlstrom BL, Michalowicz BS, Johnson NW. Periodontal diseases. Lancet 2005;366(9499):1809–20.
[2] Elangovan S, Srinivasan S, Ayilavarapu S. Novel regenerative strategies to enhance periodontal therapy outcome. Expert Opin Biol Ther 2009;9(4):399–410.
[3] Ivanovski S, Vaquette C, Gronthos S, Hutmacher DW, Bartold PM. Multiphasic scaffolds for periodontal tissue engineering. J Dent Res 2014;93(12):1212–21.
[4] Rosa V, Della Bona A, Cavalcanti BN, Nör JE. Tissue engineering: from research to dental clinics. Dent Mater 2012;28(4):341–8.
[5] Langer R, Vacanti JP. Tissue engineering. Science 1993;260(5110):920–6.
[6] Carter S-SD, Costa PF, Vaquette C, Ivanovski S, Hutmacher DW, Malda J. Additive biomanufacturing: an advanced approach for periodontal tissue regeneration. Ann Biomed Eng 2017;45(1):12–22.
[7] Gopinathan J, Noh I. Recent trends in bioinks for 3D printing. Biomater Res 2018;22:11.
[8] Ribeiro A, Blokzijl MM, Levato R, Visser CW, Castilho M, Hennink WE, et al. Assessing bioink shape fidelity to aid material development in 3D bioprinting. Biofabrication 2017;10(1):014102.
[9] Pati F, Ha D-H, Jang J, Han HH, Rhie J-W, Cho D-W. Biomimetic 3D tissue printing for soft tissue regeneration. Biomaterials 2015;62:164–75.
[10] Pati F, Jang J, Ha DH, Won Kim S, Rhie JW, Shim JH, et al. Printing three-dimensional tissue analogues with decellularized extracellular matrix bioink. Nat Commun 2014;5:3935.
[11] Yan Y, Wang X, Xiong Z, Liu H, Liu F, Lin F, et al. Direct construction of a three-dimensional structure with cells and hydrogel. J Bioact Compat Polym 2005;20(3):259–69.
[12] Yan Y, Wang X, Pan Y, Liu H, Cheng J, Xiong Z, et al. Fabrication of viable tissue-engineered constructs with 3D cell-assembly technique. Biomaterials 2005;26(29):5864–71.
[13] Zhang T, Yan Y, Wang X, Xiong Z, Lin F, Wu R, et al. Three-dimensional gelatin and gelatin/hyaluronan hydrogel structures for traumatic brain injury. J Bioact Compat Polym 2007;22(1):19–29.
[14] Zehnder T, Sarker B, Boccaccini AR, Detsch R. Evaluation of an alginate-gelatine crosslinked hydrogel for bioplotting. Biofabrication 2015;7(2):025001.
[15] Ouyang L, Yao R, Mao S, Chen X, Na J, Sun W. Three-dimensional bioprinting of embryonic stem cells directs highly uniform embryoid body formation. Biofabrication 2015;7(4):044101.
[16] Zhao Y, Yao R, Ouyang L, Ding H, Zhang T, Zhang K, et al. Three-dimensional printing of Hela cells for cervical tumor model in vitro. Biofabrication 2014;6(3):035001.
[17] Panwar A, Tan LP. Current status of bioinks for micro-extrusion-based 3D bioprinting. Molecules 2016;21(6).
[18] Wang X, Ao Q, Tian X, Fan J, Tong H, Hou W, et al. Gelatin-based hydrogels for organ 3D bioprinting. Polymers 2017;9(9).

[19] Loessner D, Meinert C, Kaemmerer E, Martine LC, Yue K, Levett PA, et al. Functionalization, preparation and use of cell-laden gelatin methacryloyl-based hydrogels as modular tissue culture platforms. Nat Protoc 2016;11(4):727–46.
[20] Fairbanks BD, Schwartz MP, Bowman CN, Anseth KS. Photoinitiated polymerization of PEG-diacrylate with lithium phenyl-2,4,6-trimethylbenzoylphosphinate: polymerization rate and cytocompatibility. Biomaterials 2009;30(35):6702–7.
[21] Monteiro N, Thrivikraman G, Athirasala A, Tahayeri A, Franca CM, Ferracane JL, et al. Photopolymerization of cell-laden gelatin methacryloyl hydrogels using a dental curing light for regenerative dentistry. Dent Mater 2018;34(3):389–99.
[22] Billiet T, Gevaert E, De Schryver T, Cornelissen M, Dubruel P. The 3D printing of gelatin methacrylamide cell-laden tissue-engineered constructs with high cell viability. Biomaterials 2014;35(1):49–62.
[23] Haase HR, Ivanovski S, Waters MJ, Bartold PM. Growth hormone regulates osteogenic marker mRNA expression in human periodontal fibroblasts and alveolar bone-derived cells. J Periodont Res 2003;38(4):366–74.
[24] Meinert C, Theodoropoulos C, Klein TJ, Hutmacher DW, Loessner D. A method for prostate and breast cancer cell spheroid cultures using gelatin methacryloyl-based hydrogels. In: Culig Z, editor. Prostate cancer: methods and protocols. New York, NY: Springer New York; 2018. p. 175–94.
[25] Sudheesh Kumar PT, Hashimi S, Saifzadeh S, Ivanovski S, Vaquette C. Additively manufactured biphasic construct loaded with BMP-2 for vertical bone regeneration: a pilot study in rabbit. Mater Sci Eng C 2018;92:554–64.
[26] Suntornnond R, Tan EYS, An J, Chua CK. A highly printable and biocompatible hydrogel composite for direct printing of soft and perfusable vasculature-like structures. Sci Rep 2017;7(1):16902.
[27] Melchels FPW, Dhert WJA, Hutmacher DW, Malda J. Development and characterisation of a new bioink for additive tissue manufacturing. J Mater Chem B 2014;2(16):2282–9.
[28] Yin J, Yan M, Wang Y, Fu J, Suo H. 3D bioprinting of low-concentration cell-laden gelatin methacrylate (GelMA) bioinks with a two-step cross-linking strategy. ACS Appl Mater Interfaces 2018;10(8):6849–57.
[29] Jungst T, Smolan W, Schacht K, Scheibel T, Groll J. Strategies and molecular design criteria for 3D printable hydrogels. Chem Rev 2016;116(3):1496–539.
[30] Nimal TR, Baranwal G, Bavya MC, Biswas R, Jayakumar R. Anti-staphylococcal activity of injectable nano tigecycline/chitosan-PRP composite hydrogel using Drosophila melanogaster model for infectious wounds. ACS Appl Mater Interfaces 2016;8(34):22074–83.
[31] Xu X, Jagota A, Peng S, Luo D, Wu M, Hui CY. Gravity and surface tension effects on the shape change of soft materials. Langmuir 2013;29(27):8665–74.
[32] Therriault D, White SR, Lewis JA. Rheological behavior of fugitive organic inks for direct-write assembly. Appl Rheol 2007;17(1), 10112-1-10112-8.
[33] Liu W, Heinrich MA, Zhou Y, Akpek A, Hu N, Liu X, et al. Extrusion bioprinting of shear-thinning gelatin methacryloyl bioinks. Adv Healthc Mater 2017;6(12).
[34] Schacht K, Jungst T, Schweinlin M, Ewald A, Groll J, Scheibel T. Biofabrication of cell-loaded 3D spider silk constructs. Angew Chem Int Ed Engl 2015;54(9):2816–20.
[35] Fedorovich NE, Schuurman W, Wijnberg HM, Prins HJ, van Weeren PR, et al. Biofabrication of osteochondral tissue equivalents by printing topologically defined, cell-laden hydrogel scaffolds. Tissue Eng C Methods 2012;18(1):33–44.
[36] Markstedt K, Mantas A, Tournier I, Martinez Avila H, Hagg D, Gatenholm P. 3D bioprinting human chondrocytes with nanocellulose-alginate bioink for cartilage tissue engineering applications. Biomacromolecules 2015;16(5):1489–96.
[37] Rutz AL, Hyland KE, Jakus AE, Burghardt WR, Shah RN. A multimaterial bioink method for 3D printing tunable, cell-compatible hydrogels. Adv Mater 2015;27(9):1607–14.
[38] Wang X, Yan Y, Pan Y, Xiong Z, Liu H, Cheng J, et al. Generation of three-dimensional hepatocyte/gelatin structures with rapid prototyping system. Tissue Eng 2006;12(1):83–90.
[39] De Clercq K, Schelfhout C, Bracke M, De Wever O, Van Bockstal M, Ceelen W, et al. Genipin-crosslinked gelatin microspheres as a strategy to prevent postsurgical peritoneal adhesions: in vitro and in vivo characterization. Biomaterials 2016;96:33–46.
[40] Irvine SA, Agrawal A, Lee BH, Chua HY, Low KY, Lau BC, et al. Printing cell-laden gelatin constructs by free-form fabrication and enzymatic protein crosslinking. Biomed Microdevices 2015;17(1):16.
[41] Smith CM, Stone AL, Parkhill RL, Stewart RL, Simpkins MW, Kachurin AM, et al. Three-dimensional bioassembly tool for generating viable tissue-engineered constructs. Tissue Eng 2004;10(9–10):1566–76.
[42] Das S, Pati F, Choi Y-J, Rijal G, Shim J-H, Kim SW, et al. Bioprintable, cell-laden silk fibroin–gelatin hydrogel supporting multilineage differentiation of stem cells for fabrication of three-dimensional tissue constructs. Acta Biomater 2015;11:233–46.
[43] Duchi S, Onofrillo C, O'Connell CD, Blanchard R, Augustine C, Quigley AF, et al. Handheld co-axial bioprinting: application to in situ surgical cartilage repair. Sci Rep 2017;7(1):5837.